Dynamics of Endoergic Bimolecular Proton Transfer Reactions: $F^- + ROH \rightarrow HF + RO^-$ ($R = H$, CH_3, CH_3CH_2, $(CH_3)_2CH$, and $(CH_3)_3C$)

Vincent F. DeTuri, Moon A. Su, and Kent M. Ervin*

Department of Chemistry and Chemical Physics Program, University of Nevada, Reno, Nevada 89557

Received: October 23, 1998; In Final Form: December 30, 1998

Guided ion beam tandem mass spectrometry techniques are used to measure reaction threshold energies for proton transfer of water, methanol, ethanol, 2-propanol, and 2-methyl-2-propanol with fluoride anion, $F^- + ROH \rightarrow RO^- + HF$, where R = H, CH_3, CH_3CH_2, $(CH_3)_2CH$, or $(CH_3)_3C$. The measured reaction threshold energy is an upper limit for the gas-phase acidity of the alcohol relative to hydrogen fluoride. Our guided ion beam measurements yield threshold energies that are consistently higher than those based on current literature gas-phase acidity values by 5−9 kJ/mol, indicating that the reactions have a small effective barrier in excess of the endoergicity. To help interpret the experiments, ab initio and density functional theory techniques are used to calculate the proton transfer reaction potential energy surfaces. No intrinsic barriers or double minima along the reaction path are found on the potential energy surfaces. Possible dynamical bottlenecks for translational activation are discussed in detail.

I. Introduction

Although proton transfer reactions have been studied for many years, there are remaining issues about the kinetics, mechanisms, and energetics of the proton transfer reactions, including whether they proceed on single-well or double-well potential energy surfaces.[1−7] Exothermic proton transfer reactions proceed at or near the collision rate,[8,9] implying no barriers to proton transfer. Studies of thermoneutral proton transfer reactions show reaction efficiencies less than the expected 50%,[10−12] however, which does imply either a potential energy or dynamical barrier. In this work, guided ion beam techniques are used to study the translational activation of endoergic bimolecular proton transfer reactions between fluoride anion and water or a series of alcohols.

By studying the energetics of proton transfer reactions between two species, a relative gas-phase acidity may be determined. Gas-phase acidities can be used to derive important intrinsic molecular properties, such as carbon−hydrogen bond dissociation energies and hydrocarbon radical enthalpies of formation.[13] These quantities are important for understanding and modeling combustion processes.[14,15] Reliable gas-phase acidity measurements can be made by measuring the proton transfer equilibrium with a well-known reference acid,[13] preferably as a function of temperature. Suitable reference acids, or "anchors" to the gas-phase acidity scale, are usually those for which the gas-phase acidity value is obtained by a thermochemical cycle based on a spectroscopic bond dissociation energy, the radical electron affinity, and the ionization energy of hydrogen, $\Delta_{acid}H(RH) = D(R-H) - EA(R) + IE(H)$.

An alternative method for obtaining a gas-phase acidity is to measure the threshold energy for an endoergic proton transfer reaction.[16−22] In this work, reaction 1 is studied using guided ion beam tandem mass spectrometry.

$$F^- + ROH \rightarrow RO^- + HF,\ R = H,\ CH_3,\ CH_3CH_2,\ (CH_3)_2CH,\ \text{or}\ (CH_3)_3C \quad (1)$$

The measured 0 K reaction threshold energy for reaction 1, E_0, is equal to the reaction enthalpy, Δ_rH_0, in the absence of any potential barriers along the reaction path or any dynamical barriers hindering proton transfer. If any barriers are present, the measured reaction threshold energy is an upper limit to the true reaction enthalpy, as shown in eq 2 for reaction 1.

$$E_0 \geq \Delta_rH_0 = \Delta_{acid}H_0(ROH) - \Delta_{acid}H_0(HF) \quad (2)$$

The results we obtain are compared with literature gas-phase acidity values, to test the validity of our experimental protocol using guided ion beam techniques.

The series of alcohols in reaction 1 was chosen as a test system because the gas-phase acidities of these alcohols have been studied for over 28 years,[23] the reactions are relatively simple (i.e., no steric hindrance or resonance effects), and the systems are treatable by ab initio and DFT methods. Table 1 shows the gas-phase acidities in this series of alcohols measured by various techniques. The absolute experimental gas-phase acidities have risen over a number of years, but relative values are fairly constant. Our evaluation of literature values will be discussed in detail. Another reason to study these alcohols is that the gas-phase acidities, from methanol to 2-methyl-2-propanol (*tert*-butyl alcohol), fall near the well-known anchor acids, HF, HCCH, and H_2O (Table 2). Fluoride anion was chosen as the proton transfer reagent because of the well-known gas-phase acidity of HF and because fluoride reacts endothermically with all the alcohols studied here.

We find that our measured reaction threshold energies are only upper limits to the reaction enthalpies, with apparent barriers of 5−9 kJ/mol. Several aspects of the gas-phase proton-transfer reactions that could explain apparent barriers are examined. In particular, barriers along the potential energy surface and dynamical impediments along the proton transfer reaction path are considered and also discussed in the context of exothermic and thermoneutral reactions.

II. Methods

A. Bimolecular Proton Transfer Experiments. Experiments were carried out using our guided ion beam tandem mass

* Corresponding author. E-mail: ervin@chem.unr.edu.

10.1021/jp9842392 CCC: $18.00
Published on Web 02/17/1999

TABLE 1: Summary of Literature Values of Gas-Phase Acidities, $\Delta_{acid}H_{298}$ (kJ/mol), for a Series of Alcohols[a]

method	ref (year)	CH_3OH	CH_3CH_2OH	$(CH_3)_2CHOH$	$(CH_3)_3COH$
ICR[b]	24,25 (1979)	1592 ± 9	1579 ± 9	1571 ± 9	1567 ± 9
HPMS[c]	26 (1986)	1597 ± 3			
pyrolysis[d,e]	27 (1987)	1596 ± 3[f]	1584 ± 4[g]	1574 ± 5[h]	1568^{+5}_{-7}[h]
SIFT[i]	28 (1990)			1578 ± 3	1575 ± 3
kinetic[j]	29 (1993)	1595 ± 8	1582 ± 8	1572 ± 8	1566 ± 8
PTS[d,k]	30 (1995)	1600 ± 2[f]			
reanchored[l]		**1600 ± 2**	**1587 ± 3**	**1579 ± 3**	**1575 ± 3**
ab initio[m]	this work	1602	1585	1575	1569

[a] Values in boldface type are used to compare with our measured reaction threshold energies. [b] Ion cyclotron resonance. Values have been altered from the original reference[24] due to changes in the acidity scale.[25] [c] High-pressure mass spectrometry. [d] $D-EA$, $\Delta_{acid}H_{298}(RH) = D_{298}(R-H) - EA_{298}(R) + IE(H)$, where $IE(H)^{31} = 1312.0496 \pm 0.0010$ kJ/mol, using the EA specified in footnotes. [e] Review of pyrolysis kinetics. [f] $EA_0(CH_3O) = 151.3 \pm 0.5$ kJ/mol, ref 32. [g] $EA_0(CH_3CH_2O) = 165.5 \pm 0.7$ kJ/mol, ref 33. [h] $EA_0((CH_3)_2CHO) = 177.4 \pm 2.8$ kJ/mol and $EA_0((CH_3)_3CO) = 184.5^{+2.8}_{-5.2}$ kJ/mol, ref 34. [i] Selected ion flow tube kinetics. These values have been increased by +2 kJ/mol from the original reference based on a more recent precise measurement of $D_0(HCCH)$.[35] [j] Cooks kinetic method. [k] Photofragment translational spectroscopy of $CH_3O \rightarrow CH_3 + O$. [l] ICR values[24,25] reanchored to the gas-phase acidity of methanol determined by photofragment translational spectroscopy.[30] The errors bars from the reanchored ICR scale were calculated from propagating the ICR relative acidity measurement error of ±0.8 kJ/mol, the estimated entropy error of ±5 J mol^{-1} K^{-1}, and the photofragment translation spectroscopy error in the gas-phase acidity of methanol of ±2 kJ/mol. [m] MP2/6-311++G(d,p)//MP2/6-31G(d), thermal correction to 298 K using eq 4.

TABLE 2: Summary of Literature Thermochemical Values (kJ/mol)

species (R−H)	EA_0 (R)	D_0 (R−H)[a]	$\Delta_{acid}H_0(RH)$[a]	$\Delta_{acid}H_{298}(RH)$[b]	ab initio[c]
HO−H	176.3419 ± 0.0020[d]	494.1 ± 0.2[e]	1629.8 ± 0.2	1634.7 ± 0.2	1634
HCC−H	287 ± 1[f]	551.2 ± 0.1[g]	1577 ± 1	1583 ± 1	1581
F−H	328.1649 ± 0.0004[h]	566.6 ± 0.8[e]	1550.4 ± 0.8	1554.2 ± 0.8	1553

[a] $\Delta_{acid}H(RH) = D(R-H) - EA(R) + IE(H)$, where $IE(H)^{31} = 1312.0496 \pm 0.0010$ kJ/mol. [b] Thermal correction from eq 4. [c] $\Delta_{acid}H_{298}$, MP2/6-311++G(d,p)//MP2/6-31G(d), with a thermal correction to 298 K using eq 4. [d] Reference 36. [e] Reference 37. [f] Reference 28. [g] Reference 35. [h] Reference 38.

spectrometer, which is described in detail elsewhere.[39] Briefly, fluoride anions are created in a flow tube reactor using a microwave discharge source with helium buffer gas and hexafluorobenzene as a precursor gas. Fluoride anion, isoelectronic with neon, has no low-lying excited electronic states that necessitate cooling. A magnetic sector mass spectrometer is used to mass select F^-. After mass selection, the ions are injected into an octopole ion beam guide where they collide with the neutral reactant, water, methanol, ethanol, 2-propanol, or 2-methyl-2-propanol. All the alcohols are spectroscopic grade and used without further purification except degassing. Reactant and product ions are extracted from the octopole region and mass analyzed with a quadrupole mass spectrometer.

Absolute reaction cross sections are determined as a function of collision energy between the reactants; a thorough discussion has been presented previously.[39,40] Briefly, reactant and product ion intensities are recorded as a function of collision energy, from which a reaction cross section is calculated. The laboratory ion energy is measured using retarding potential analysis, confirmed by time-of-flight,[39] and is then converted to the relative collision energy, E, in the center-of-mass (c.m.) frame.[40] To obtain absolute reaction cross sections in the absence of multiple collisions, the data are collected at three different pressures and extrapolated to zero pressure. The zero pressure extrapolated cross section, $\sigma(E)$, is modeled[41] using an empirical threshold law,[39,40,42] eq 3,

$$\sigma(E) = \sigma_0 \sum_i g_i[E + E_i - E_0]^N/E \qquad (3)$$

where E_i is the internal energy of reactant state i with fractional thermal population g_i corresponding to a Maxwell−Boltzman distribution at 300 K, σ_0 and N are adjustable parameters, and E_0 is the 0 K reaction threshold energy. The rovibrational density of states is calculated using the Beyer−Swinehart Stein−Rabinovitch direct count algorithm.[43−45] Finally, eq 3 is convoluted over the collision energy distribution of the reactants, as described elsewhere.[40] For some reactions, a nonzero cross section is observed at low energies resulting from translationally trapped ions in the octopole. These translationally trapped ions are removed by pulsing the ion beam and the octopole trapping field, as described previously.[39] The data were collected using various pulse timing sequences, which had no effect on the shape of the cross sections. The ion beam pulsing imposes a lower energy limit of 0.02−0.1 eV, c.m., depending on reactant masses.[39]

The error bars quoted on our threshold energies are propagated from individual sources of uncertainty (assuming they are independent of each other) and represent estimates of $\pm 2\sigma$, or about the 95% confidence limit. We include the uncertainties from determination of the ion beam energy zero, the least-squares fit to the data, the molecular parameters used in the model, the reproducibility of data taken on separate occasions, and the consistency of the model fit using different energy ranges. The absolute cross section magnitudes are correct to ±50%.

B. Theoretical Methods. Calculations were performed using Gaussian 94.[46] For the internal energy distribution in eq 3, vibrational frequencies and rotational constants in Table 3 were calculated at the Hartree−Fock level using the 6-31G(d) basis set; vibrational frequencies were scaled by 0.8953.[47] Previous work on anionic proton transfer systems shows that electron correlation and diffuse basis sets are necessary to obtain realistic results for energies.[3,5,49−53] To find the best level and methodology for the proton transfer systems studied in this paper, we calculated gas-phase acidities (enthalpies of deprotonation at 0 K) for several test systems (H_2O, CH_3OH, HCCH, and HF), examining treatment of electron correlation, and basis set size, from geometries optimized at the MP2/6-31G(d) level with higher level energy calculations. Gas-phase acidities were also calculated at the G2[54] and G2(MP2)[55] levels. Table 4 lists the mean absolute deviations of the computed gas-phase acidities from literature values. Within a target accuracy of ±3 kJ/mol,

TABLE 3: Rotational Constants and Vibrational Frequencies (cm^{-1})[a]

	HO[b]	HO^-[b]	H_2O[b]
rotation	18.87	19.2	27.89, 14.51, 9.28
vibration	3735.21	3770	1594.4, 3651.1, 3755.9
	CH_3O	CH_3O^-	CH_3OH
rotation	5.36, 0.92, 0.92	5.34, 0.93, 0.93	4.24, 0.82, 0.79
vibration	727, 993, 1086, 1418, 1427, 1491, 2849, 2908, 2926	1157, 1173, 1173, 1443, 1443, 1503, 2318, 2318, 2458	283, 1020, 1065, 1156, 1340, 1459, 1475, 1476, 2845, 2894, 2915, 3669
	CH_3CH_2O	$CH_3CH_2O^-$	CH_3CH_2OH
rotation	1.20, 0.34, 0.30	1.27, 0.33, 0.29	1.16, 0.30, 0.26
vibration	235, 381, 400, 871, 873, 984, 1108, 1231, 1341, 1390, 1456, 1472, 1515, 2866, 2882, 2901, 2946, 2952	286, 404, 745, 792, 1014, 1163, 1188, 1244, 1332, 1393, 1442, 1454, 1491, 2329, 2426, 2760, 2829, 2853	240, 282, 398, 789, 870, 1008, 1084, 1156, 1242, 1267, 1379, 1436, 1450, 1465, 1500, 2826, 2848, 2859, 2916, 2927, 3662
	$(CH_3)_2CHO$	$(CH_3)_2CHO^-$	$(CH_3)_2CHOH$
rotation	0.31, 0.27, 0.16	0.31, 0.27, 0.17	0.29, 0.27, 0.16
vibration	197, 240, 334, 343, 443, 785, 878, 903, 954, 1069, 1078, 1173, 1267, 1315, 1384, 1405, 1456, 1461, 1467, 1478, 2839, 2868, 2876, 2925, 2933, 2944, 2946	233, 270, 335, 406, 468, 729, 802, 850, 977, 1058, 1119, 1203, 1315, 1335, 1341, 1354, 1440, 1448, 1449, 1467, 2381, 2762, 2777, 2826, 2836, 2860, 2865	215, 256, 294, 344, 397, 463, 787, 901, 917, 957, 1048, 1133, 1164, 1247, 1351, 1370, 1396, 1410, 1449, 1454, 1462, 1472, 2818, 2844, 2858, 2896, 2911, 2919, 2926, 3653
	$(CH_3)_3CO$	$(CH_3)_3CO^-$	$(CH_3)_3COH$
rotation	0.17, 0.17, 0.15	0.16, 0.16, 0.15	0.16, 0.16, 0.15
vibration	192, 233, 250, 305, 318, 374, 391, 422, 714, 878, 896, 905, 941, 972, 1011, 1208, 1210, 1244, 1385, 1386, 1412, 1449, 1457, 1461, 1469, 1469, 1489, 2869, 2874, 2882, 2926, 2933, 2939, 2940, 2946, 2947	210, 264, 264, 315, 315, 381, 450, 450, 668, 784, 784, 875, 986, 986, 993, 1165, 1165, 1249, 1335, 1335, 1352, 1437, 1445, 1445, 1455, 1455, 1471, 2769, 2769, 2789, 2839, 2839, 2852, 2861, 2872, 2872	204, 258, 264, 298, 323, 325, 397, 441, 446, 712, 886, 896, 929, 933, 1004, 1021, 1131, 1230, 1231, 1330, 1385, 1391, 1407, 1442, 1451, 1452, 1463, 1470, 1482, 2841, 2847, 2861, 2893, 2901, 2915, 2917, 2924, 2926, 3645

[a] From HF/6-31G(d) calculations, unless otherwise noted. Calculated vibrational frequencies have been scaled by 0.8953.[47] [b] JANAF thermochemical tables.[48]

TABLE 4: Comparison of Theoretical and Experimental Gas-Phase Acidities, $\Delta_{acid}H_0$[a]

		theory − exptl[b] (kJ/mol)				MAD[c]
method	basis set	H_2O	CH_3OH	HCCH	HF	(kJ/mol)
HF	6-31G(d)	127	68	73	135	101
	6-311+G(d,p)	32	32	2	15	20
B3LYP	6-31G(d)	139	47	76	172	109
	6-311+G(d,p)	−10	−14	−9	−18	13
MP2	6-31G(d)	127	107	76	145	114
	6-31G(d,p)	153	75	93	177	125
	6-311G(d,p)	144	64	46	139	98
	6-311+G(d,p)	−1	3	−2	−2	2
	6-311++G(d,p)	−1	2	−2	−2	2
	6-311G(2df,p)	129	45	34	126	84
	6-311+G(2df,p)	−11	−12	−10	−10	11
	6-311+G(3df,2p)	−14	−11	−10	−9	11
MP4D	6-31G(d)	133	64	79	148	106
	6-311+G(d,p)	24	24	6	19	18
QCISD(T)	6-31G(d)	134	57	108	150	112
	6-311+G(d,p)	13	13	1	10	9
G2(MP2)		−2	2	−4	3	3
G2		−4	1	−3	2	3

[a] Energies calculated from optimized MP2/6-31G(d) geometry, and ZPE corrections from scaled (0.8953) HF/6-31G(d) frequencies. [b] Experimental values at 0 K taken from Tables 1 and 2. [c] Mean absolute deviation.

the following methods did the best job: MP2/6-311+G(d,p), MP2/6-311++G(d,p), G2(MP2), G2. For larger alcohol systems, all stationary points were calculated at the MP2/6-311++G(d,p)//MP2/6-31G(d) level with scaled[47] HF/6-31G(d) zero-point energy (ZPE) corrections.

Potential energy surface and reaction path curvature[56] calculations were performed for the $F^- + H_2O$ system. Electron correlation may play a significant role in defining the minimum energy path. Without compromising much accuracy, an intrinsic reaction coordinate (IRC) was calculated at the B3LYP/6-311+G(d,p) level.

III. Proton Transfer Measurements

A. Guided Ion Beam Results. In this section, we present our guided ion beam results and threshold fits.

1. Pressure Dependence. As the $F^- + ROH$ reaction proceeds, a transient $ROHF^-$ collision complex forms. In the absence of multiple collisions with the reactant gas, this complex will either form products or fall back to reactants. Collisions between the transient complex and the reactant gas can lead to stabilization of an adduct by removing excess energy. Adduct formation is prevalent for the larger systems because of the increased polarizability and high number of vibrational degrees of freedom, leading to long lifetimes at low energies, but essentially nonexistent in the water and methanol reactions. Figure 1 shows adduct formation for the $F^- + (CH_3)_3COH$ reaction at a high and low gas cell pressure. Also shown in Figure 1 is the extrapolation to zero pressure for the $(CH_3)_3CO^-$ and $(CH_3)_3COHF^-$ product channels at two different energies. The apparent cross section for the $(CH_3)_3CO^-$ product shows a linear pressure dependence implying a contribution from a second collision. A linear extrapolation of the $(CH_3)_3CO^-$ channel to zero pressure gives the absolute bimolecular reaction cross section under single-collision conditions.[39] The apparent

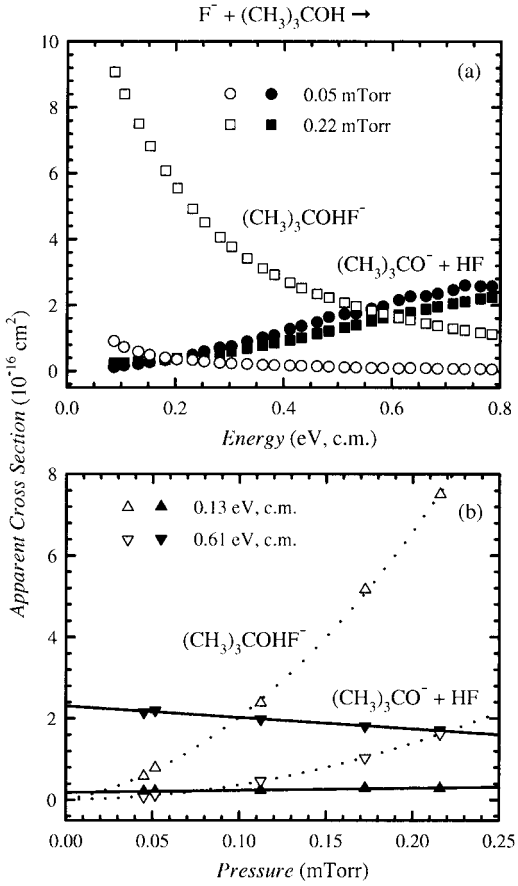

Figure 1. (a) Apparent reaction cross sections for formation of $(CH_3)_3CO^-$ (solid symbols) and the $(CH_3)_3COHF$ (open symbols) from $F^- + (CH_3)_3COH$ at two pressures as a function of energy. (b) Zero-pressure extrapolation showing cross section as a function of pressure for two energies.

cross section for the $(CH_3)_3COHF^-$ product channel shows a quadratic pressure dependence, implying multiple collisions. A quadratic zero-pressure extrapolation on the $(CH_3)_3COHF^-$ adduct goes to zero cross section, within experimental uncertainty. Therefore, adduct detection is purely an artifact of multiple collision conditions. All further cross sections reported here are extrapolated to zero pressure, and only single-collision bimolecular reaction processes are reported.

2. Reaction Threshold Energies. Cross sections for reaction 1 are presented in Figures 2−4. Reaction threshold energies were obtained by fitting the reaction cross sections to the convoluted empirical threshold law, eq 3. From these reaction threshold energies, an upper limit for the gas-phase acidity of the alcohol is obtained relative to the gas-phase acidity of HF (Table 2) using eq 2. Table 5 gives a summary of the results. The conversion from 0 to 298 K is given by eq 4, where the heat capacities, $C_P(T)$, are calculated using the molecular parameters in Table 3 in the rigid-rotor harmonic-oscillator approximation using standard statistical mechanics formulas.[57]

$$\Delta_r H_{298} = \Delta_r H_0 + \int_0^{298} \Delta_r C_P(T)\, dT \qquad (4)$$

a. Methanol, Ethanol, and 2-Propanol. The fits of eq 3 to the methanol, ethanol, and 2-propanol cross sections are excellent, as shown in Figure 2. The 0 K GIB threshold energies are reported in Table 5 along with the best values for σ_0 and N.

b. 2-Methyl-2-propanol. Our single-collision cross section result, shown in Figure 3, for $F^- + (CH_3)_3COH$ shows a nonzero

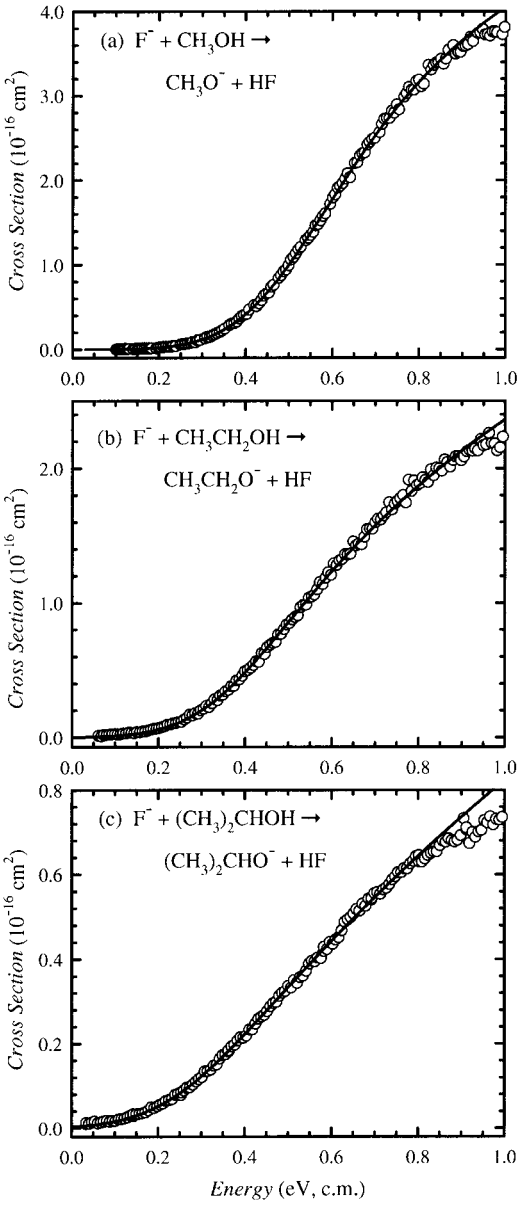

Figure 2. Single-collision cross sections for reaction of fluoride anion with (a) methanol, (b) ethanol, and (c) 2-propanol. Solid lines show the fits to the data described in text.

cross section at the lowest energies. This feature is due to the thermal population of internal energy levels in 2-methyl-2-propanol above the 0 K endoergicity. At 300 K, 26% of the internal population is above the literature 0 K threshold energy of 19.7 kJ/mol for the reaction. This low-energy cross section feature was modeled with a Langevin cross section for ion-induced dipole capture,[58,59] scaled (by about 0.5%) to match the cross section at lowest energies, and subtracted before fitting the threshold. Similar modeling procedures have been described previously.[60,61] Figure 3 shows the fit to the data with the Langevin cross section added in. The error bars of the threshold energy in Table 5 reflect the extra uncertainty based on the subtraction procedure.

c. Water. Figure 4 shows the single-collision cross section for reaction 1 with ROH = HOH. The convoluted cross section model could fit the data in the threshold region, but overall the fit is poor especially near the falloff region (>0.8 eV). We tried to model this high-energy falloff behavior using methods described by Armentrout and co-workers,[62] but that model did not fit the data appreciably better. Overall, the reaction cross

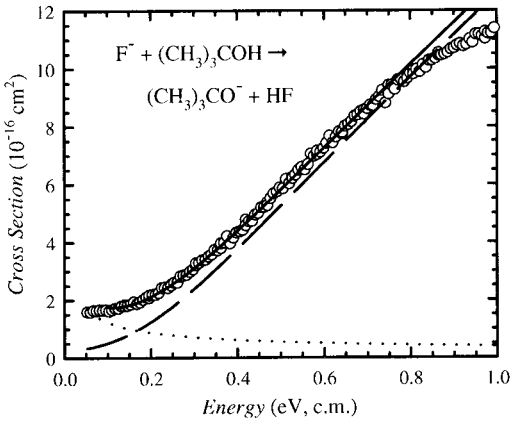

Figure 3. Single-collision reaction cross section for proton transfer of fluoride anion with 2-methyl-2-propanol. The dotted line shows the Langevin cross section scaled by about 0.5%. The dashed line shows the best fit of the Langevin subtracted data as described in text. The solid line is the sum of the dashed and dotted lines.

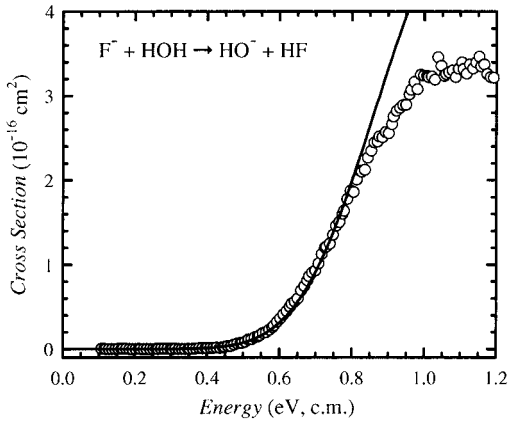

Figure 4. Single-collision reaction cross section for proton transfer of fluoride anion with water. Solid line shows the fit to the data described in text.

section was difficult to fit compared with the alcohols. The cross section rises sharply at 0.6 eV then quickly plateaus near 1.0 eV. This behavior gives low values of *N*, and for some fits *N* went negative. Fits with *N* below 0.1 were discarded. The difficulty of fitting implies that our threshold model is inadequate for this system. Using a step function, hard-sphere limit, as a model and convoluting that over our reactant energies also gave a poor fit to the data. We also modeled the data using classical phase space theory;[63] this model did a very poor job of fitting the data. The large error bar for the threshold energy in Table 5 reflects the poor quality of the fit using eq 3.

B. Evaluation of Literature Acidities. A summary of the literature gas-phase acidity values is given in Table 1, where the values in boldface type are used to compare with our measured reaction threshold energies.

1. Ion Cyclotron Resonance (ICR). The ICR values originally reported by McIver and co-workers[24] have been updated by Bartmess[25] to reflect changes in the acidity scale. The gas-phase acidity ladder was constructed with HF as a nearby anchor point. However, only $(CH_3)_3CCH_2OH$, 2,2-dimethyl-1-propanol was measured directly to HF with a relative acidity difference of 2.1 ± 0.8 kJ/mol (0.5 ± 0.2 kcal/mol, as originally reported). All other acidities were determined by some connection to $(CH_3)_3CCH_2OH$. The following compounds were measured relative to each other: $(CH_3)_3COH$ to $(CH_3)_3CCH_2OH$; $(CH_3)_2CHOH$ to $(CH_3)_3COH$; CH_3CH_2OH to $(CH_3)_2CHOH$; CH_3OH to CH_3CH_2OH. An advantage of the gas-phase acidity ladder is that there are several checks for most gas-phase acidities, and the relative differences between the acidities of closely related species, for example, this series of alcohols, are reliable. The ICR equilibrium measurements are made at 600 K requiring a correction to thermal energies, and an entropy correction[24] is necessary to find the enthalpies of deprotonation.

2. High-Pressure Mass Spectrometry (HPMS). HPMS[26] was used to measure the gas-phase acidity of methanol relative to water, by a van't Hoff temperature-dependent equilibrium measurement. The reported gas-phase enthalpy difference is 40 $\pm$ 1 kJ/mol (9.6 ± 0.2 kcal/mol) at 600 K. This value gives a gas-phase acidity 5 kJ/mol higher than the ICR study. The HPMS measurement employs a temperature-dependent equilibrium and should therefore give a more reliable gas-phase acidity.

3. Thermochemical Cycle. If the hydrocarbon bond dissociation energy and the radical electron affinity are well-known, it is better to use eq 5 to calculate the gas-phase acidity.

$$\Delta_{acid}H(\mathrm{ROH}) = D(\mathrm{RO{-}H}) - \mathrm{EA(RO)} + \mathrm{IE(H)} \quad (5)$$

The electron affinities of the radicals in this series of alcohols have been measured by negative ion photoelectron spectroscopy.[32−34] Accurate bond dissociation energies can be found by measuring enthalpies of formation for the radical, RO, the alcohol, ROH, and hydrogen. The hydrogen enthalpy of formation is 1312.0496 $\pm$ 0.0010 kJ/mol,[31] and the ROH enthalpies of formation are well-known,[25] so the difficulty is obtaining reliable and accurate values for the radical enthalpy of formation. The enthalpies of formation of the RO radicals are taken from a review of pyrolysis kinetics experiments compiled by Batt.[27] Batt finds that the RO−H dissociation energies in this series of alcohols are very similar, varying by only 5 kJ/mol. Therefore, the variation in gas-phase acidities is mainly a result of the variation of electron affinities of the radical. There are three recent $D_0(CH_3O{-}H)$ values in the literature[30,64,65] since the review by Batt.[27] Ruscic and Berkowitz[64] reviewed the pyrolysis data of Batt and co-workers and recommend $\Delta_f H_0(CH_3O) = 25 \pm 4$ kJ/mol (5.9 ± 1 kcal/mol), which yields $D_0(CH_3O{-}H) = 431 \pm 4$ kJ/mol and $\Delta_{acid}H_{298}(CH_3$-

TABLE 5: Threshold Fits at 0 K for $F^- + ROH \rightarrow RO^- + HF$

ROH species	lit[a] E_0 (eV)	all vibrations[b] σ_0	all vibrations[b] N	all vibrations[b] E_0 (eV)	OH only[c] E_0 (eV)	no rot[d] E_0 (eV)	no int[e] E_0 (eV)
H_2O	0.822 ± 0.008	9.8	0.33	0.88 ± 0.11	0.88	*f*	*f*
CH_3OH	0.465 ± 0.024	3.12	0.84	0.523 ± 0.030	0.507	0.461	0.385
CH_3CH_2OH	0.332 ± 0.033	4.62	1.58	0.390 ± 0.046	0.364	0.328	0.244
$(CH_3)_2CHOH$	0.243 ± 0.033	1.39	1.65	0.329 ± 0.048	0.218	0.267	0.118
$(CH_3)_3COH$	0.206 ± 0.033	16.5	1.89	0.28 ± 0.10	0.12	0.23	0.04

[a] Calculated from literature values in Tables 1 and 2 and converted to 0 K using eq 4 and parameters in Table 3. [b] Summation in eq 3 over all internal vibrations and overall molecular rotations. [c] Summation in eq 3 over the OH stretch, bend, and torsion, and overall molecular rotations, only. Values were corrected to 0 K. [d] No molecular rotations were considered in eq 3. [e] No internal energies were considered in eq 3, but the resulting E_{298} value was corrected to E_0. [f] *N* goes negative.

OH) = 1597 ± 4 kJ/mol. Wittig and co-workers[65] measured the translational energy release spectra of photodissociated CH_3O-H and obtain $D_0(CH_3O-H) = 439 \pm 4$ kJ/mol (105 ± 1 kcal/mol), resulting in $\Delta_{acid}H_{298}(CH_3OH) = 1605 \pm 4$ kJ/mol. Neumark and co-workers[30] using photofragment translational spectroscopy report $D_0(CH_3-O) = 367 \pm 1$ kJ/mol (87.8 ± 0.3 kcal/mol). From this value, Neumark and co-workers derive $\Delta_fH_0(CH_3O) = 28 \pm 2$ kJ/mol (6.8 ± 0.5 kcal/mol) and $D_0(CH_3O-H) = 435 \pm 2$ kJ/mol (104.0 ± 0.5 kcal/mol), which yields $\Delta_{acid}H_{298}(CH_3OH) = 1600 \pm 2$ kJ/mol. These three independently derived 298 K gas-phase acidities are within mutual uncertainties. Averaging the three values together gives $\Delta_{acid}H_{298}(CH_3OH) = 1600 \pm 2$ kJ/mol, which is the same as the value from Neumark and co-workers.[30,32] We recommend this value as the most reliable value for the absolute gas-phase acidity of methanol.

4. Selected Ion Flow Tube (SIFT). The acidity of acetylene was measured relative to 2-propanol and 2-methyl-2-propanol using SIFT kinetics.[28] A direct equilibrium was not measured; instead, the forward and reverse reaction rates were measured independently. A precise value for the bond dissociation energy of acetylene has since been reported,[35] allowing an updated gas-phase acidity for acetylene (Table 2). This newer acetylene gas-phase acidity can be used to recalculate the gas-phase acidities of 2-propanol and 2-methyl-2-propanol, giving an increase of +2 kJ/mol from the originally reported values, which is reflected in Table 1. The SIFT values are 7−8 kJ/mol higher than the previous ICR results. We recommend the SIFT values for the gas-phase acidity of 2-propanol and 2-methyl-2-propanol because the SIFT experiments provide values that are more directly related to a reliable reference compound than the ICR values. The flow tube values might be suspect by 1−2 kJ/mol because of a simplification in the entropy determination,[24] but that is well within the given uncertainties and is also present in the other equilibrium studies.

5. Cooks Kinetic Method. An alternative method to equilibrium measurements is the Cooks kinetic method,[29] in which the branching ratio is measured for the collision-induced fragmentation of proton-bound cluster ions at 50 eV. This method estimates the gas-phase acidities of the alcohols relative to 2-propanol using a linear free energy relationship. However, the authors include methanol, ethanol, and 2-methyl-2-propanol as calibration compounds, using ICR equilibrium data compiled by Lias et al.[66] Therefore, these experiments are not independent measurements of the *absolute* gas-phase acidities but do reaffirm the reliability of the *relative* gas-phase acidity measurements in the ICR scale for this series of alcohols.

6. Selected Values. When comparing the ICR gas-phase acidity of methanol to the other independent gas-phase acidity measurements, it is apparent that the ICR scale is slightly off. However, the relative gas-phase acidities of the alcohols should still be reliable. This prompted us to reanchor the ICR scale to the most recent gas-phase acidity of methanol from the bond energy of Neumark and co-workers.[30] The reanchoring appears in Table 1 as the bold entries. When comparing the methanol bond dissociation energy of Batt[27] to the value of Neumark and co-workers,[30] there is an increase of 4 kJ/mol. From the reanchoring of the ICR scale to the newest gas-phase acidity value of methanol, the bond dissociation energy of ethanol increases by 3 kJ/mol. This suggests that the pyrolysis kinetics[27] measurements slightly underestimate the bond dissociation energies in this series of alcohols. The reanchored ICR scale is in excellent agreement with the independent SIFT gas-phase acidities for 2-propanol and 2-methyl-2-propanol. This agreement further supports the reliability of the relative values in the ICR scale between closely related species and our reanchoring of the ICR scale. We select the reanchored values as the most reliable absolute gas-phase acidities.

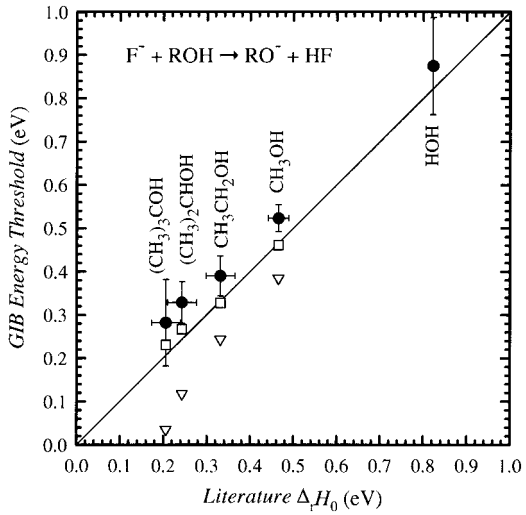

Figure 5. Comparison of GIB energy threshold results vs literature values at 0 K, for reaction 1: (Solid circles) E_0 from summation in eq 3 over all internal vibrations and overall molecular rotations; (open sqares) summation over molecular vibrations only; (open triangles) E_0 with no internal energies considered. For clarity the error bars appear only for the solid circles but are identical for each model.

7. Ab Initio. Calculations at the MP2/6-311++G(d,p)//MP2/6-31G(d) level with a scaled HF/6-31G(d) ZPE correction were performed to compute gas-phase acidities for this series of alcohols. Table 1 also lists the results from these calculations with a correction to 298 K using eq 4. The ab initio calculated gas-phase acidities agree well with the reanchored values.

C. Comparison with Selected Literature Values. On the basis of the analysis above, the reanchored values of the ICR scale were chosen for comparison with our proton transfer threshold energies. Figure 5 and Table 5 compare our results with these selected literature values, converted into 0 K threshold energies for reaction 1 using eqs 2 and 4. Our GIB threshold energies, solid circles, are systematically higher than previous literature values by 5−9 kJ/mol; if our results agreed with previous literature, the circles would fall on the line in Figure 5. Although the deviations from literature values are small, they are systematic and are outside of our conservative error bars for methanol, ethanol, and 2-propanol.

IV. Discussion

Possible reasons for the 5−9 kJ/mol systematic discrepancy between the GIB values and previous literature values include an error in our fitting procedure, an energetic barrier, a dynamical barrier, or perhaps that the selected literature values are in error. The literature values for this series of alcohols have increased over the years (Table 1), but the reanchored ICR gas-phase acidity scale is reliable and shows good agreement among independent methods. Furthermore, new results we have obtained using competitive collision-induced dissociation of proton bound complexes such as $(ROH)F^-$ support the reliability of the reanchored ICR values.[67] Therefore, we believe the 5−9 kJ/mol deviation represents an issue in translationally activated bimolecular proton transfer or the analysis procedure. Further discussion of the fitting procedures and reaction path energetics and dynamics appears below.

A. Internal Energy. Typically, the threshold data are fit including all the vibrations and rotations of the reactants in eq

3. This assumes that all modes of energy equally promote the proton transfer, which is reasonable for a transient ion−molecule complex that decomposes statistically.[60,68−70] Treating the OH torsion as a free rotor, rather than as a harmonic vibration, lowered our measured gas-phase acidities by 1 kJ/mol. Although it would be best to treat the OH torsion as a hindered rotor, the two extremes (harmonic oscillator or free rotor) differ by only 1 kJ/mol, not accounting for the 5−9 kJ/mol deviation with previous literature values.

Another possibility is that not all of the internal vibrations of the neutral alcohol participate in the reaction. If no rotational and vibrational energy is included as taking part in the reaction, the resulting threshold energy represents[71] $E_{298} = \Delta_r H_{298}$. We correct these values to $E_0 = \Delta_r H_0$ using eq 4. The resulting values, listed in Table 5 and shown as triangles in Figure 5, move significantly lower than the literature values, by 7−16 kJ/mol. (The water value is missing because N becomes negative resulting in a pathological fit to the data.) These results confirm that at least most of the internal energy of the reactant molecule is available to promote the proton transfer reaction. Graul and Squires[20] did not include internal energy in eq 3 to model their thresholds for endoergic proton transfer of HO^-, CH_3O^-, and $C_2H_5O^-$ with C_2H_4. Their reported threshold energies are systematically 7−17 kJ/mol lower than expected from current thermochemistry (Tables 1 and 2, and NIST[25]). Although within their reported uncertainties of 10−20 kJ/mol, these deviations suggest that internal energy is available to promote those proton transfer reactions also.

If including all the internal vibrations gives values too high and not including any internal vibrations gives values too low, then the correct treatment of internal vibrations might lie somewhere in between. The vibrations that should participate the most in the reaction will be the OH vibrations. The alcohols were also fit with only the OH stretch, bend, and torsion, and overall molecular rotations included as active. The resulting reaction enthalpies (Table 5) are systematically lower than our previous values including all the internal vibrations. The methanol and ethanol gas-phase acidities are still higher than literature values, but the 2-propanol and 2-methyl-2-propanol gas-phase acidities are lower. Since this method of only including the OH vibrations does not work for all systems, there is no indication that vibrational promotion of the reactions is mode-specific and no expectation that this method would work for an unknown system. For the water system, taking out all the vibrations or including only the symmetric OH stretch gave the same poor fits to the cross-section data.

Keeping all vibrational modes active but excluding rotational energy lowers E_0 by about 6 kJ/mol. This offset gives good agreement between the GIB E_0 and the literature values (Table 5 and squares in Figure 5). The literature does not provide firm guidance on whether rotational energy should be included. Armentrout and co-workers[60,68] studying the hydrogen abstraction bimolecular reactions of $C^+ + H_2$ and $N^+ + H_2$ and Tosi et al.[72] studying $N^+ + D_2$ definitively show that rotational energy is available for these reactions. Unfortunately, there are no literature studies for polyatomic ion−molecule reactions that can validate the exclusion or inclusion of rotational energy by precise independent thermochemistry. For collision-induced dissociation of transition metal carbonyl anions, Squires and co-workers[73] treat the internal rotational energy as separately conserved. They argue that the internal rotational energy of an activated complex is not available for reaction and must be conserved to conserve angular momentum. The total angular momentum is equal to the vector sum of the orbital angular momentum and rotational angular momentum, $\mathbf{J} = \mathbf{L} + \mathbf{j}$. Usually L is much larger than j, so small changes in $\mathbf{L}$ should be able to compensate for changes in $\mathbf{j}$ in a bimolecular reaction. Therefore, we consider inclusion of rotational energy in the reaction coordinate as an open question for our bimolecular proton transfer reactions between fluoride anion and an alcohol. That is, the agreement obtained by removing rotational energy in eq 3 could be fortuitous. Preliminary results in our laboratory for the proton transfer between HCC^- and H_2O give a GIB threshold energy that agrees with the literature gas-phase acidity with all internal modes included in the model. Trajectory calculations using a reasonable multidimensional potential energy surface might be able to address this issue.

B. Single versus Double Well Potentials. There has been much discussion of whether the proton transfer minimum energy reaction path has a single well or a double well separated by a barrier.[1−7] Presence of a barrier, even if below the energy of the reactants or products, could reduce the reaction efficiency.[56] Some of the theoretical proton transfer studies treat systems where the distance between the proton donor and acceptor is fixed, which may be reasonable for some biological systems but does not apply to gas-phase reactions. For a gas-phase proton-bound species, a strong hydrogen bond gives a single well potential, and a weaker hydrogen bond gives a double well potential.[1−3] Emsley gives a list of guidelines defining what is a strong or weak hydrogen bond.[1] The following are three of Emsley's conditions for a strong hydrogen bond as applied to $ROHF^-$: the H−F vibrational stretch should be below 1600 cm^{-1}, the complexation energy should be greater than 50 kJ/mol, and the O−F distance should be significantly less than the sum of the van der Waals radii, where $r(F) = 1.40$ Å and $r(O) = 1.50$ Å. For all the alcohols studied here, the H−F vibrational stretch (from scaled HF/6-31G(d) calculations) is around 300 cm^{-1}, and from ab initio geometry optimizations, the O−F distance is around 2.4 Å, significantly less than the sum of the van der Waals radii[1] of 2.9 Å. The $ROHF^-$ complexation energy is around 120 kJ/mol for this series of alcohols and water,[74] well above the complexation energy guideline reported by Emsley. Scheiner[4] has also shown that for XHX^- systems strong hydrogen bonds are observed for species where the X···X distance is 2.4 Å or less. This implies a strong hydrogen bond between the alcohols and fluoride anion and suggests there should only be a single well along the reaction path.

Ab initio studies on symmetric anionic systems[3] also show that only a single well exists along the proton transfer reaction pathway when there is strong hydrogen bonding. For the FHF^- system, there is only one well; the F−F distance is 2.28 Å, the H−F vibrational stretch is 616 cm^{-1}, and the well depth[75] is 192 ± 7 kJ/mol. For the $HOHOH^-$ system, there is also only one well, when zero-point energy is included.[3] This system also follows the guidelines of Emsley[1] (the vibrational frequency is 1082 cm^{-1}, the O−O bond length is 2.44 Å, and the well depth from experimental measurements[76] is 112 ± 4.2 kJ/mol). Two systems that show a double well are $H_2NHNH_2^-$ (experimental well depth[77] is 50.2 kJ/mol) and $H_3CHCH_3^-$. Both species have weak hydrogen bonding.[3] These strong versus weak hydrogen bond results can be explained by acidity strength and electronegativies; F^- and OH^- are both very electronegative and are stronger bases than NH_2^- and CH_3^-.

Neumark and co-workers[5] studied the potential energy suface of CH_3OHF^- looking for a $CH_3O^-\cdot HF$ minimum separate from the $CH_3OH\cdot F^-$ minimum. The O−F distance for CH_3OHF^- at the MP2/6-311++G(d,p) level is 2.432 Å. Starting with this

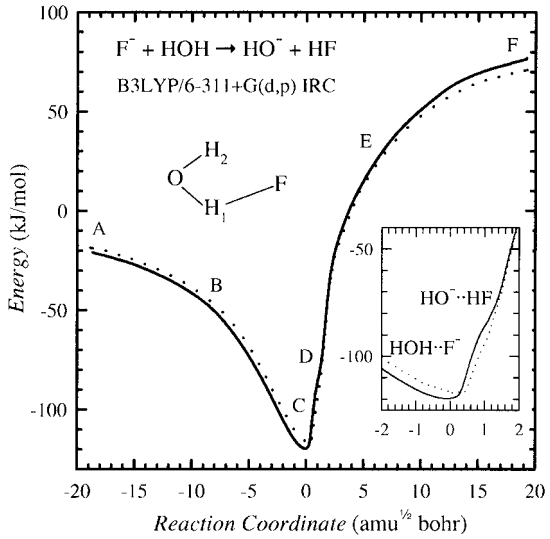

Figure 6. Intrinsic reaction coordinate for $F^- + H_2O \rightarrow HO^- + HF$ plotted in mass weighted internal coordinates. Labels A−F refer to selected geometries listed in Table 6; (solid) potential surface; (dotted) potential surface plus a ZPE correction, both energies relative to reactants. The inset plot is an expanded view of the surface around the bottom of the well.

minimized geometry and constraining all degrees of freedom except for the proton position between O and F, Neumark and co-workers tried to find a $CH_3O^-{\cdot}HF$ minimum. No second minimum was found, but there was a relatively flat region around the minimum rather than a parabolic surface. Photoelectron spectroscopy of CH_3OHF^- also supports a surface with one minimum.[5−7]

Figure 6 shows the intrinsic reaction coordinate (IRC) for the $F^- + H_2O \rightarrow HO^- + HF$ minimum energy path, which we calculated at the B3LYP/6-311+G(d,p) level including a ZPE correction. These results are consistent with those of Xantheas and co-workers,[51] who examined the same system at the MP4/aug-cc-pVTZ level of theory. The reaction surface shows the long-range ion−dipole attraction in the entrance channel, then a steep descent to the minimum, where the geometry is F^- associated with water, $HOH{\cdot}F^-$. There is a small inflection and a steep exit channel as the complex leaves the minimum and proceeds to products. The geometry of the complex at the inflection is more like HF associated with HO^-, i.e., $HO^-{\cdot}HF$. Geometries at selected points along the reaction path are shown in Table 6. The path to products from this inflection rises steeply then mirrors the entrance channel except for the higher asymptotic energy. Figure 6 clearly shows that there is a single well potential with no intrinsic barriers on the potential energy surface. Pérez and co-workers[53] also studied the $F^- + H_2O \rightarrow HO^- + HF$ reaction and obtained a double well potential but with the O−F distance artificially constrained to 2.9 Å. On the basis of our optimized $F^- + H_2O$ calculations, Figure 6, and the $F^- + CH_3OH$ surface,[5−7] we expect the larger alcohols to have similar single-well surfaces, with no intrinsic potential energy barriers in either the entrance or exit channel. Thus, the experimentally observed barriers are not due to potential energy barriers.

C. Kinetics Evidence. Exothermic ion−molecule proton transfer reactions are typically fast, near the collision rate, except for species with charge delocalization and steric hindrance, implying there is no overall barrier for proton-transfer reactions.[8,9,11] However, Bouchoux and co-workers[78] using ICR experiments to study cationic proton transfer reactions see apparent Gibbs free energy barriers of 4.8 ± 0.4 kJ/mol for near-thermoneutral reactions, at temperatures near 500 K.

To examine the issue of kinetic barriers in exothermic anionic proton transfer reactions further, we have compiled literature data on reaction efficiencies. Table 7 lists the experimental rate constants for a series of proton transfer reactions taken from a 1986 compilation.[79] We include all the anionic proton transfer reactions in ref 79 that are exergonic ($\Delta_r G_{298} < 0$)[25] and for which the ion-polar capture rates are calculable from polarizabilities and dipole moments in ref 81. Capture rates constants, k_{cap}, obtained from parametrized classical trajectories,[80] and reaction efficiencies, k_{exp}/k_{cap}, are given in Table 7, as are activation energies, $E^{\ddagger}_{act}$, estimated by eq 6.

$$E^{\ddagger}_{act} = -RT \ln(k_{exp}/k_{cap}) \qquad (6)$$

Most of the exergonic reactions are nearly 100% efficient with no activation barrier. Deviations from this are probably due to inaccuracies in the theoretical capture rate constants or small errors in the experimental rate constants. The only reaction that shows an appreciable activation barrier and a lowered reaction efficiency is $F^- + (CH_3)_3CCH_2OH \rightarrow (CH_3)_3CCH_2O^- + HF$. However, this is probably a result of the slight endothermicity of the reaction,[25] $\Delta_r H_{298} = 5 \pm 9$ kJ/mol. Overall, Table 7 shows that for exergonic and exothermic proton transfer systems there is no kinetic activation barrier. Microscopic reversibility would imply that the corresponding endothermic reactions should proceed with no excess barriers, but that strictly applies only for the same state-to-state reaction in each direction.

Kinetic studies on exactly thermoneutral proton transfer identity reactions between alkoxide anions and neutral alcohols, in constrast to the exothermic reactions, show reaction efficiencies lower than the expected 50%.[11] For reaction 7, reaction efficiencies of 26−35% have been reported.[10−12]

$$CH_3O^- + HOCH_3 \leftrightarrow [H_3COHOCH_3]^- \leftrightarrow CH_3OH + {}^-OCH_3 \qquad (7)$$

Using eq 6, that implies an apparent activation energy of 2.6−3.4 kJ/mol. This is consistent with Bouchoux and co-workers[78] and slightly less than the effective barriers we find for endothermic proton transfer. Assuming a double well potential for reaction 7 and using a RRKM model, Brauman and co-workers[11] found an apparent barrier of 74.5 kJ/mol relative to the complex (the complex minimum is 123 kJ/mol below

TABLE 6: Geometries of Selected Points in the IRC Calculation for $F^- + H_2O \rightarrow HO^- + HF$

point[a]	complex	R(O−H$_2$)	R(O−H$_1$)	ϕ(H−O−H)	R(H$_1$−F)	ϕ(O−H$_1$−F)
A	$F^- + H_2O$	0.97	0.96	106	5.00	121
B	$HOH{\cdots}F^-$	0.96	0.97	100	3.50	140
C	$HOH{\cdot}F^-$	0.96	1.06	102	1.40	175
D	$HO^-{\cdot}HF$	0.96	1.31	108	1.21	179
E	$HO^-{\cdots}HF$	0.97	3.62	120	0.93	180
F	$HO^- + HF$	0.97	5.00	180	0.93	180

[a] See Figure 6. The complex remains planar for the entire reaction path.

TABLE 7: Rate Constant Data for a Series of Proton Transfer Reactions near 300 K[a]

$X^- + RH \rightarrow R^- + XH$	k_{exp}[a] (10^{-9} cm^3/s)	k_{cap}[b] (10^{-9} cm^3/s)	% RE[c]	$\Delta_r G_{300}$[d] (kJ/mol)	$E^{\ddagger}_{act}$ (kJ/mol)
$F^- + (CH_3)_3CCH_2OH$	0.29	2.8	10	−0.5(9)	5.7
$C_2H_5O^- + C_2H_2$	1.4(25%)	1.1	130(40)	−7(5)	−0.6(0.7)
$CH_3O^- + C_2H_5OH$	3.3(1.0)	2.3	140(50)	−10(10)	−0.9(0.8)
$HO^- + CH_3OH$	2.2(0.6)	2.8	79(26)	−13(8)	0.6(0.6)
$CH_3O^- + (CH_3)_3COH$	1.1	2.3	48	−20(9)	1.8
$HO^- + C_2H_5OH$	2.7(0.8)	2.8	96(32)	−23(8)	0.1(0.6)
$HO^- + C_2H_5OH$	2.2(0.7)	2.8	78(32)	−23(8)	0.6(0.6)
$HO^- + C_2H_2$	2.2(0.4)	1.3	170(30)	−31.1(2.5)	−1.3(0.5)
$NO_2^- + HCl$	1.4(30%)	1.5	93(31)	−57.3(1.3)	0.2(0.6)
$NO_2^- + HBr$	1.9(30%)	1.1	170(60)	−64.4(1.4)	−1.4(0.8)
$NO^- + HCl$	1.6(30%)	1.6	100(30)	−150(5)	0.0(0.7)
$F^- + HCl$	1.55(0.31)	1.9	82(18)	−191.6(1.3)	0.5(0.3)
$F^- + HI$	1.01(0.20)	1.6	63(14)	−236.8(1.5)	1.1(0.5)

[a] Taken from ref 79. Uncertainties in parentheses. [b] Rate constants from parametrized classical trajectories.[80] Dipole moments and molecular polarizabilities from ref 81. [c] Reaction efficiency, k_{exp}/k_{cap}. [d] Relative gas-phase acidity differences from ref 25.

reactants) along the proton transfer reaction surface, explaining these slow rates. McMahon and co-workers[12] also attribute the slow reaction efficiency of reaction 7 to a barrier along the proton transfer reaction surface, i.e., a double well potential. However, a potential energy barrier is not consistent with the calculated potential energy surface for reaction 7.[82] Also, ab initio surfaces for proton transfer between two strong electronegative atoms show no barriers exist along the bottom of the well in excess of 4 kJ/mol.[83] Therefore, the lower than 50% reaction efficiencies must be explained by dynamical effects rather than an energy barrier.

D. Dynamical Effects. Although no intrinsic potential energy barriers appear on the calculated reaction path surfaces, there could be dynamical barriers or bottlenecks along the proton transfer reaction pathway. Dynamical barriers might be caused by centrifugal expansion of the O−F distance creating a barrier,[6,49,53,84] by nonrandomization of internal energies because of a rotationally locked transition state,[6,11] or by high curvature along the reaction path.[56]

1. Centrifugal Effects. It has been suggested that centrifugal distortion of the O−F distance caused by high total angular momentum could create a potential barrier along the reaction path.[6,49,53,84] Lim and Brauman[85] studied the thermoneutral reaction 7; they found that values of $J > 400\hbar$ lead to a rotationally enhanced barrier along the proton transfer reaction path due to elongation of the O−O distance. Lim and Kier[86] report that the average J value for these proton transfer reactions is $150\hbar$, at thermal energies. For the endothermic reactions, we find maximum values of $L < 100\hbar$ based on the maximum impact parameter consistent with the measured cross sections. A centrifugal distortion calculation[87] shows that $J = 100\hbar$ would not increase the O−F distance more than 0.02 Å, too little to create a proton transfer barrier. Thus, centrifugal effects do not seem to be an issue in our experiment.

2. Rotationally Locked Transition State. Lim and Brauman[82] proposed that the slow rates of reaction 7 could be explained by a "rotationally locked transition state" (RLTS) model. Before complexation occurs in reaction 7, the methyl group on methanol is considered a free rotor. As complexation occurs, the free rotor is converted into a hindered rotor and finally into a vibrational bending mode. Lim and Brauman propose that this lowering of the density of states creates a bottleneck along the reaction path, preventing the complex from randomizing its internal energies. However, our ab initio calculations using the method described by Radom and co-workers[88] show formation of a $ROHF^-$ complex actually lowers the barrier height for internal rotation. Therefore, the RLTS model does not seem appropriate for reaction 1.

3. Nonstatistical Energy Redistribution. A nonrandomization of the internal energies of the collision complex could lead to a dynamical bottleneck slowing down the rate of reaction 7 or could lead to a small barrier to proton transfer for reaction 1. Trajectory calculations of reaction 7 using a model XHX system in one dimension were done by Hinde and Ezra,[89] excluding all angular considerations. If the reactants first form a complex, where the internal energies become completely random, the reaction efficiency is 50%. For a direct reaction, where the internal energies are not allowed to randomize, the reaction efficiency is only 15%. The apparent barrier along the reaction path is from this nonrandomization of internal energies and is purely dynamical in nature. Hence, this barrier to proton transfer will not appear in potential energy calculations and cannot be modeled by statistical theory. McMahon and co-workers[12] using ICR techniques find the reaction efficiency for an $[CH_3CH_2OHOCH_2CH_3]^-$ system is near 37%, whereas for $[(CH_3)_2CHOHOCH(CH_3)_2]^-$ and $[(CH_3)_3COHOC(CH_3)_3]^-$ the reaction efficiency is 47%. The increase in reaction efficiency could result from better randomization of internal energy for systems with more degrees of freedom and longer complex lifetimes. However, our results show that most vibrational energy is available to promote reaction 1, regardless of the size of the alcohol, but are consistent with some internal rotational energy being excluded. The one-dimensional trajectory calculations[89] do not address rotational effects.

4. Reaction Path Curvature. Trajectory calculations by Wang and Hase[56] for the $Cl^- + CH_3Br \rightarrow ClCH_3 + Br^-$ S_N2 reaction may offer insight into our proton transfer reaction dynamics. The S_N2 reaction may be viewed as a CH_3^+ transfer reaction, similar to proton transfer, but the proton transfer systems have a single well potential rather than the double well potential with a high central barrier observed for S_N2 reactions.[90−93] Wang and Hase showed for S_N2 reactions that the curvature of the reaction path results in inefficient energy transfer between translational energy and energy available to promote reaction. High reaction path curvature tends to reflect reactants from forming products.

Figure 6 shows our ab initio calculations for the $F^- + H_2O$ proton transfer reaction pathway. To determine the curvature along the reaction path, ab initio vibrational analyses were done at points along the minimum energy path. Also shown in Figure 6 is the ZPE-corrected potential energy (adjusted relative to the reactant energies) calculated from the vibrational frequencies

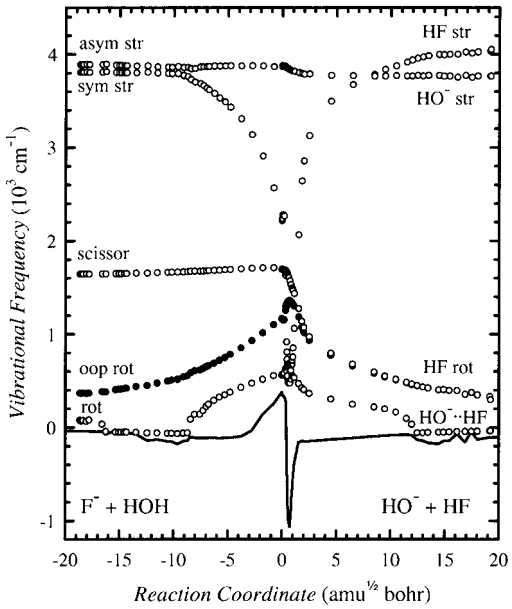

Figure 7. Harmonic frequencies along the reaction path. The solid line is the reaction coordinate.

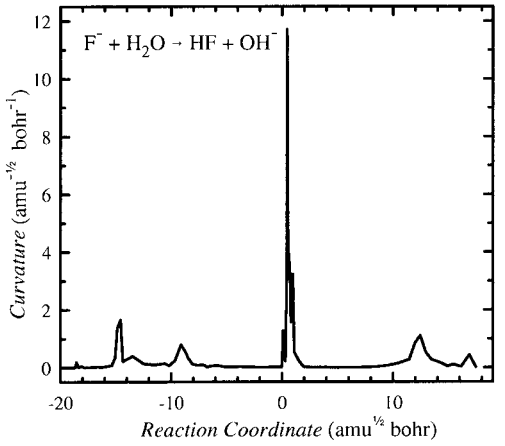

Figure 8. Reaction path curvature along the reaction coordinate.

along the surface. Figure 7 shows harmonic vibrational frequencies along the reaction path at the B3LYP/6-311+G(d,p) level. The rapid changes in frequencies along the reaction path imply that complex motions are required. The coupling of each vibrational mode to the reaction coordinate was calculated using eq 3 from ref 56. We assign the most negative vibrational frequency as the reaction path. The reaction path curvature is calculated using eq 4 from ref 56. Instead of generating a reaction path Hamiltonian from an analytic potential energy function as Wang and Hase describe, we use discrete points along the reaction path to calculate the necessary derivatives numerically. This limits our analysis of the coupling terms and curvature (about 100 points were calculated) and introduces some noise into the calculation, but major features are reliable.

As shown in Figure 8, there are several regions of high curvature along the reaction path that may limit the transfer of translational energy to promote product formation. The first area of high curvature is in the entrance channel as the fluoride anion begins to associate preferentially with one of the hydrogens on water rather than being aligned with the overall dipole moment of water. Physically, the long-range ion−dipole potential orients the reactants in a direction that is not most favorable at short range. The point of highest curvature along the reaction path is just after the bottom of the well near the inflection point where the complex changes character from $HOH{\cdot}F^-$ to $HO^-{\cdot}HF$. In the exit channel, the last area of high curvature is where the complex dissociates and begins to behave as two independent diatomic molecules with a dipole−dipole interaction. Each of these regions of high curvature represents a possible impediment to efficient reaction and could therefore induce an apparent barrier for translational activation. The curvature effects are likely most extreme for $F^- + H_2O$, consistent with the unusual threshold behavior observed, but could persist for the alcohols. Thus, reaction path curvature effects provide a plausible explanation for the small effective barriers observed, but more detailed theoretical analysis would be required to quantify this effect.

V. Conclusions

Bimolecular endoergic proton transfer reactions have been studied experimentally using guided ion beam techniques and by theoretical methods. Our measured proton transfer threshold energies are systematically higher than the literature gas-phase acidity differences by 5−9 kJ/mol, but the relative values for the alcohols are consistent with the relative ICR values.[24] This work finds that there are no intrinsic potential energy barriers along the proton transfer reaction pathway, but there may be dynamical barriers. Dynamical barriers could arise either from an inability of molecular rotational energy to promote the reaction or from high curvature along the reaction path, preventing efficient translational-to-internal energy transfer between F^- and the alcohol. The importance of rotational energy and reaction path curvature could be tested by trajectory calculations on a reasonable multidimensional potential energy surface.

Apparent barriers for the $F^- + ROH$ systems may be a special case. The underlying chemical reason for dynamical barriers might be because fluoride ion is possibly, in retrospect, a poor choice as a proton acceptor. Fluoride anion is a closed-shell species isoelectronic with Ne, with a small atomic radius, making it a hard base.[94,95] The low polarizability of F^- may reduce the interaction time and result in poor energy transfer. Our proton transfer reaction threshold for $Cl^- + C_6H_5OH$ gave reasonable agreement with literature values,[22] possibly because Cl^- is a more diffuse anion, giving a longer interaction time. Our preliminary results for proton transfer between HCC^- and H_2O also give the correct value for the reaction enthalpy, perhaps because of the more diffuse nature of acetylide, π-bonding effects, or because both reactants are polyatomic.

Until the barrier issue is resolved by theoretical dynamics studies or precise thermochemical comparisons in additional polyatomic reaction systems, proton transfer threshold energies from translational activation should be treated as providing upper limits for gas-phase acidities. We note that the errors observed, 5−9 kJ/mol, are reasonably small compared with uncertainties for many gas-phase acidities.[13] Therefore, the endoergic bimolecular proton-transfer method is still useful in cases where other methods are not applicable, if for example the conjugate base anion is unstable or difficult to produce for equilibrium studies. An alternative method of measuring accurate gas-phase acidities using guided ion beam techniques involves first making the thermal $ROHF^-$ complex. The $ROHF^-$ complex can be activated in a collision-induced dissociation experiment, where there will be a competition between the $ROH + F^-$ and the $RO^- + HF$ product channels. The difference in energy thresholds between these two channels can be correlated with the gas-phase acidity of ROH relative to HF. Our results from such experiments show excellent agreement with literature values and will be published shortly.[67]

Acknowledgment. The authors would like to thank Professor William L. Hase for helpful discussions about the reaction path curvature effects and Professor Peter B. Armentrout for discussions of internal energy effects. This research is supported by the Department of Energy, Basic Energy Sciences, Grant DE-FG03-97ER14750. Undergraduate Senior Thesis research by M.A.S. was supported by the DOE/Nevada EPSCoR Young Scholars Program.

References and Notes

(1) Emsley, J. *Chem. Soc. Rev.* **1980**, *9*, 91−124.
(2) Scheiner, S. *J. Mol. Struct. (THEOCHEM)* **1994**, *307*, 65−71.
(3) Gronert, S. *J. Am. Chem. Soc.* **1993**, *115*, 10258−10266.
(4) Latajka, Z.; Scheiner, S.; Chalasinski, G. *Chem. Phys. Lett.* **1992**, *196*, 384−389.
(5) Bradforth, S. E.; Arnold, D. W.; Metz, R. B.; Weaver, A.; Neumark, D. M. *J. Phys. Chem.* **1991**, *95*, 8066−8078.
(6) Wladkowski, B. D.; East, A. L. L.; Mihalick, J. E.; Allen, W. D.; Brauman, J. I. *J. Chem. Phys.* **1994**, *100*, 2058−2088.
(7) Mihalick, J. E.; Gatev, G. G.; Brauman, J. I. *J. Am. Chem. Soc.* **1996**, *118*, 12424−12431.
(8) Guo, Y.; Grabowski, J. J. *Int. J. Mass Spectrom. Ion Processes* **1990**, *97*, 253−264.
(9) Grabowski, J. J. In *Advances in Gas-Phase Ion Chemistry*; Adams, N. G., Babcock, L. M., Eds.; JAI Press: Greenwich, CT, 1992; pp 43−81.
(10) Barlow, S. E.; Dang, T. T.; Bierbaum, V. M. *J. Am. Chem. Soc.* **1990**, *112*, 6832−6838.
(11) Dodd, J. A.; Baer, S.; Moylan, C. R.; Brauman, J. I. *J. Am. Chem. Soc.* **1991**, *113*, 5942−5949.
(12) Wilkinson, F. E.; Peschke, M.; Szulejko, J. E.; McMahon, T. B. *Int. J. Mass Spectrom. Ion Processes* **1998**, *175*, 225−240.
(13) Berkowitz, J.; Ellison, G. B.; Gutman, D. *J. Phys. Chem.* **1994**, *98*, 2744−2765.
(14) Liñán, A.; Williams, F. A. *Fundamental Aspects of Combustion*; Oxford: New York, 1993.
(15) Dryer, F. L. In *Fossil Fuel Combustion: A Source Book*; Bartok, W., Sarofim, A. F., Eds.; John Wiley & Sons: New York, 1991; pp 121−213.
(16) Hughes, B. M.; Lifshitz, C.; Tiernan, T. O. *J. Chem. Phys.* **1973**, *59*, 3162−3181.
(17) Refaey, K. M. *J. Chem. Phys.* **1976**, *64*, 4810−4811.
(18) Refaey, K. M. *J. Chem. Phys.* **1976**, *65*, 2002−2006.
(19) Huq, M. S.; Fraedrich, D. S.; Doverspike, L. D.; Champion, R. L.; Esaulov, V. A. *J. Chem. Phys.* **1982**, *76*, 4952−4960.
(20) Graul, S. T.; Squires, R. R. *J. Am. Chem. Soc.* **1990**, *112*, 2517−2529.
(21) Lee, H. S.; Bierbaum, V. M. *J. Chem. Phys.* **1994**, *101*, 9513−9518.
(22) DeTuri, V. F.; Ervin, K. M. *Int. J. Mass Spectrom.* **1998**, *175*, 123−132.
(23) Brauman, J. I.; Blair, L. K. *J. Am. Chem. Soc.* **1970**, *92*, 5986−5992.
(24) Bartmess, J. E.; Scott, J. A.; McIver, R. T., Jr. *J. Am. Chem. Soc.* **1979**, *101*, 6046−6056.
(25) Bartmess, J. E. In *NIST Standard Reference Database Number 69*; Mallard, W. G., Linstrom, P. J., Eds.; National Institute of Standards and Technology, 1997 (http://webbook.nist.gov).
(26) Meot-Ner (Mautner), M.; Sieck, L. W. *J. Phys. Chem.* **1986**, *90*, 6687−6690.
(27) Batt, L. *Int. Rev. Phys. Chem.* **1987**, *6*, 53−90.
(28) Ervin, K. M.; Gronert, S.; Barlow, S. E.; Gilles, M. K.; Harrison, A. G.; Bierbaum, V. M.; DePuy, C. H.; Lineberger, W. C.; Ellison, G. B. *J. Am. Chem. Soc.* **1990**, *112*, 5750−5759.
(29) Haas, M. J.; Harrison, A. G. *Int. J. Mass Spectrom. Ion Processes* **1993**, *124*, 115−124.
(30) Osborn, D. L.; Leahy, D. J.; Ross, E. M.; Neumark, D. M. *Chem. Phys. Lett.* **1995**, *235*, 484−489.
(31) Moore, C. E. *Atomic Energy Levels*; National Standard Reference Data Series: National Bureauof Standards (US), 1971; Vol. 1.
(32) Osborn, D. L.; Leahy, D. J.; Kim, E. H.; de Beer, E.; Neumark, D. M. *Chem. Phys. Lett.* **1998**, *292*, 651−655.
(33) Dang, T. T.; Motell, E. L.; Travers, M. J.; Clifford, E. P.; Ellison, G. B.; DePuy, C. H.; Bierbaum, V. M. *Int. J. Mass Spectrom. Ion Processes* **1993**, *123*, 171−185.
(34) Ellison, G. B.; Engelking, P. C.; Lineberger, W. C. *J. Phys. Chem.* **1982**, *86*, 4873−4878.
(35) Mordaunt, D. H.; Ashfold, M. N. *J. Chem. Phys.* **1994**, *101*, 2630−2631.
(36) Schulz, P. A.; Mead, R. D.; Jones, P. L.; Lineberger, W. C. *J. Chem. Phys.* **1982**, *77*, 1153−1165.
(37) *Thermodynamic Properties of Individual Substances*, 4th ed.; Gurvich, L. V., Veyts, I. V., Alcock, C. B., Eds.; Hemisphere Publishing Corporation: New York, 1989.
(38) Blondel, C.; Cacciani, P.; Delsart, C.; Trainham, R. *Phys. Rev. A* **1989**, *40*, 3698−3701.
(39) DeTuri, V. F.; Hintz, P. A.; Ervin, K. M. *J. Phys. Chem. A* **1997**, *101*, 5969−5986 and references therein.
(40) Ervin, K. M.; Armentrout, P. B. *J. Chem. Phys.* **1985**, *83*, 166−189.
(41) Armentrout, P. B.; Ervin, K. M. *CRUNCH*; Fortran program.
(42) Rodgers, M. T.; Ervin, K. M.; Armentrout, P. B. *J. Chem. Phys.* **1997**, *106*, 4499−4508.
(43) Beyer, T. S.; Swinehart, D. F. *Commun. ACM* **1973**, *16*, 379.
(44) Stein, S. E.; Rabinovitch, B. S. *J. Chem. Phys.* **1973**, *58*, 2438−2445.
(45) Stein, S. E.; Rabinovitch, B. S. *Chem. Phys. Lett.* **1977**, *49*, 183−188.
(46) Frisch, M. J.; Trucks, G. W.; Schlegel, H. B.; Gill, P. M. W., et al. *Gaussian94*, Revision D.4; Gaussian, Inc.: Pittsburgh, 1995.
(47) Scott, A. P.; Radom, L. *J. Phys. Chem.* **1996**, *100*, 16502−16513.
(48) Chase, M. W., Jr.; Davies, C. A.; Downey, J. R., Jr.; Frurip, D. J.; McDonald, R. A.; Syverud, A. N. *J. Phys. Chem. Ref. Data* **1985**, *14* (Suppl. 1).
(49) Platts, J. A.; Laidig, K. E. *J. Phys. Chem.* **1996**, *100*, 13455−13461.
(50) Pudzianowski, A. T. *J. Phys. Chem.* **1996**, *100*, 4781−4789.
(51) Xantheas, S. S.; Dang, L. X. *J. Phys. Chem.* **1996**, *100*, 3989−3995.
(52) Merrill, G. N.; Kass, S. R. *J. Phys. Chem.* **1996**, *100*, 17465−17471.
(53) Pérez, P.; Contreras, R.; Vela, A.; Tapia, O. *Chem. Phys. Lett.* **1997**, *269*, 419−427.
(54) Curtiss, L. A.; Raghavachari, K.; Trucks, G. W.; Pople, J. A. *J. Chem. Phys.* **1991**, *94*, 7221−7230.
(55) Curtiss, L. A.; Raghavachari, K.; Pople, J. A. *J. Chem. Phys.* **1993**, *98*, 1293−1298.
(56) Wang, H.; Hase, W. L. *Chem. Phys.* **1996**, *212*, 247−258.
(57) Herzberg, G. *Molecular Spectra and Molecular Structure II. Infrared and Raman Spectra of Polyatomic Molecules*; Van Nostrand Reinhold: New York, 1945.
(58) Stevenson, D. P.; Schissler, D. O. *J. Chem. Phys.* **1958**, *29*, 282−294.
(59) Gioumousis, G.; Stevenson, D. P. *J. Chem. Phys.* **1958**, *29*, 292−299.
(60) Ervin, K. M.; Armentrout, P. B. *J. Chem. Phys.* **1986**, *86*, 2659−2673.
(61) Meyer, F.; Khan, F. A.; Armentrout, P. B. *J. Am. Chem. Soc.* **1995**, *117*, 9740−9748.
(62) Weber, M. E.; Elkind, J. L.; Armentrout, P. B. *J. Chem. Phys.* **1986**, *84*, 1521−1529.
(63) Aristov, N.; Armentrout, P. B. *J. Phys. Chem.* **1986**, *90*, 5135−5140.
(64) Ruscic, B.; Berkowitz, J. *J. Chem. Phys.* **1991**, *95*, 4033−4039.
(65) Wen, Y.; Segall, J.; Dulligan, M.; Wittig C. *J. Chem. Phys.* **1994**, *101*, 5665−5671.
(66) Lias, S. G.; Bartmess, J. E.; Liebman, J. F.; Holmes, J. L.; Levin, R. D.; Mallard, W. G. *J. Phys. Chem. Ref. Data* **1988**, *17* (Suppl. 1).
(67) DeTuri, V. F.; Ervin, K. M. To be published.
(68) Ervin, K. M.; Armentrout, P. B. *J. Chem. Phys.* **1984**, *80*, 2978−2980.
(69) Schultz, R. H.; Crellin, K. C.; Armentrout, P. B. *J. Am. Chem. Soc.* **1991**, *113*, 8590−8601.
(70) Armentrout, P. B.; Hales, D. A.; Lian, L. In *Advances in Metal and Semiconductor Clusters*; Duncan, M. A., Ed.; JAI Press: Greenwich, CT, 1994; Vol. 2, pp 1−39.
(71) Dalleska, N. F.; Honma, K.; Armentrout, P. B. *J. Am. Chem. Soc.* **1993**, *115*, 12125−12131.
(72) Tosi, P.; Dmitriev, O.; Bassi, D.; Wick, O.; Gerlich, D. *J. Chem. Phys.* **1994**, *100*, 4300−4307.
(73) Sunderlin, L. S.; Wang, D.; Squires, R. R. *J. Am. Chem. Soc.* **1993**, *115*, 12060−12070.
(74) Larson, J. W.; McMahon, T. B. *J. Am. Chem. Soc.* **1983**, *105*, 2944−2950.
(75) Wenthold, P. G.; Squires, R. R. *J. Phys. Chem.* **1995**, *99*, 2002−2005.
(76) Paul, G. J. C.; Kebarle, P. *J. Phys. Chem.* **1990**, *94*, 5184−5189.
(77) Snodgrass, J. T.; Coe, J. V.; Freidhoff, C. B.; McHugh, K. M.; Arnold, S. T.; Bowen, K. H. *J. Phys. Chem.* **1995**, *99*, 9675−9680.
(78) Bouchoux, G.; Salpin, J. Y.; Leblanc, D. *Int. J. Mass Spectrom. Ion Proc.* **1996**, *153*, 37−48.
(79) Ikezoe, Y.; Matsuoka, S.; Takebe, M.; Viggiano, A. *Gas-Phase Ion−Molecule Reaction Rate Constants Through 1986*; Mass Spectroscopy Society of Japan: Tokyo, 1987.
(80) Su, T.; Chesnavich, W. J. *J. Chem. Phys.* **1982**, *76*, 5183−5185.

(81) *CRC Handbook of Chemistry and Physics*, 78th ed.; Lide, D. R., Ed. CRC Press: New York, 1997
(82) Lim, K. F.; Brauman, J. I. *J. Chem. Phys.* **1991**, *94*, 7164−7180.
(83) Baer, S.; Brauman, J. I. *J. Am. Chem. Soc.* **1992**, *114*, 5733−5741.
(84) Scheiner, S. *Acc. Chem. Res.* **1985**, *18*, 174−180.
(85) Lim, K. F.; Brauman, J. I. *Chem. Phys. Lett.* **1991**, *177*, 326−330.
(86) Lim, K. F.; Kier, R. I. *J. Chem. Phys.* **1992**, *97*, 1072−1078.
(87) Bernath, P. F. *Spectra of Atoms and Molecules*; Oxford: New York, 1995.
(88) East, A. L. L.; Radom, L. *J. Chem. Phys.* **1997**, *106*, 6655−6674.
(89) Hinde, R. J.; Ezra, G. S. *Chem. Phys. Lett.* **1994**, *228*, 333−340.
(90) Brauman, J. I. *J. Mass Spectrom.* **1995**, *30*, 1649−1650.
(91) Hase, W. L. *Science* **1994**, *266*, 998−1002.
(92) Shaik, S. S.; Schlegel, H. B.; Wolfe, S. *Theoretical Aspects of Physical Organic Chemistry: The S_N2 Mechanism*; John Wiley & Sons: New York, 1992.
(93) Olmstead, W. N.; Brauman, J. I. *J. Am. Chem. Soc.* **1977**, *99*, 4219−4228.
(94) March, J. *Advanced Organic Chemistry*; John Wiley & Sons: New York, 1985.
(95) Roy, R. K.; de Proft, F.; Geerlings, P. *J. Phys. Chem. A* **1998**, *102*, 7035−7040.